THE JOURNAL OF PHYSICAL CHEMISTRY C

ARTICLE

pubs.acs.org/JPCC

Thermally Activated Processes at the Co/ZnO Interface Elucidated Using High Energy X-rays

Jacques A. Dumont,*[,†] Mac C. Mugumaoderha,[†] Jacques Ghijsen,[†] Sebastian Thiess,[‡] Wolfgang Drube,[‡] Bente Walz,[‡] Martin Tolkiehn,[‡] Dmitri Novikov,[‡] Frank M. F. de Groot,[¶] and Robert Sporken[†]

[†]Centre PMR, Facultés Universitaires Notre-Dame de la Paix, rue de Bruxelles 61, B-5000 Namur, Belgium

[‡]Deutsches Elektronen-Synchrotron (DESY), Notkestrasse 85, D-22603 Hamburg, Germany

[¶]Department of Inorganic Chemistry and Catalysis, Utrecht University, Sorbonnelaan 16, 3584 CA Utrecht, The Netherlands

ABSTRACT: A detailed picture of the thermally activated processes occurring at the Co/ZnO interface is obtained by a combination of high energy X-ray based techniques: X-ray photoelectron and absorption spectroscopies and the kinematical X-ray standing wave method. At room temperature, the growth of a few monolayers of cobalt proceeds by the nucleation of nanometer-sized clusters on the polar oxygen-terminated $(000\bar{1})$ surface of a ZnO single crystal. Progressive annealing from 600 to 970 K allows separating the various interfacial reactions. At the lowest annealing temperature, Co clusters coalesce while keeping their metallic character. Above 700 K Co^0 is gradually oxidized to Co^{2+} and a thin Co rich (Zn,Co)O layer is formed. It is observed that rock salt CoO phases may form at the surface when the initial Co thickness exceeds 1 nm. At the highest annealing temperature (970 K), Co diffuses deeper into ZnO and Zn vacancies are created at subsurface sites that were previously occupied by Co.

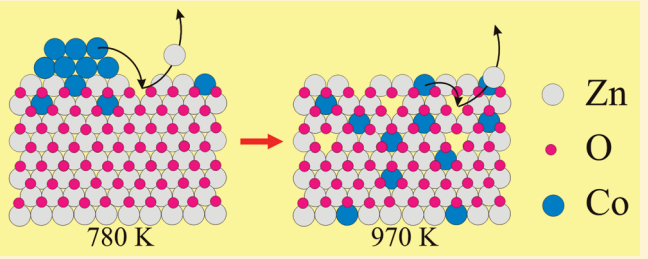

INTRODUCTION

Most thermodynamic and transport phenomena that are important for technological applications depend on the electronic and chemical properties of buried interfaces. Conventional X-ray photoelectron spectroscopy (XPS) is a key method to study the complex chemistry of solid surfaces. However, its ability to probe electronic properties below the surface is very limited due to the rather short electron escape depth. This limitation can be overcome by using considerably higher-energy photons in XPS, which offers the ability to gain a clearer understanding of the chemical and electronic properties of interfaces several nanometers below the surface. Additionally, it is often desirable to know the crystal symmetry and binding coordination of atoms of interest. This can be achieved by combining high-energy XPS with X-ray absorption near-edge spectroscopy (XANES) and kinematical X-ray standing wave (KXSW) techniques.

ZnO based materials constitute the building blocks of many actual and potential future technologies. Metal (especially Cu) particles grown on ZnO are excellent catalysts.[1] (Zn,TM)O ternary compounds where TM is a transition metal, are room temperature diluted magnetic semiconductors (DMS) and can possibly be used for spin current injection in spintronic devices.[2] Promising technological breakthrough in the field of ultrahigh density data storage as well as high speed electronics may emerge from the two-dimensional electron gas (2-DEG) at the interface between oxides such as ZnO and (Zn,Mg)O.[3]

The goal of this work is 2-fold: at first, we aim at contributing to a deeper understanding of the structural and electronic properties of the Co/ZnO system. Very recently, thermal oxidation and diffusion of Co into polar ZnO surfaces was demonstrated;[4,5] nevertheless, it is still unclear whether Co^{2+} is incorporated into a CoO secondary phase or is located in substitutional sites in the ZnO wurtzite lattice. In the present work, XPS is used both to probe the chemical reactions between Co and ZnO and, in particular, the oxidation of Co and to monitor the spatial distribution of Co, Zn, and O in the surface region as well as the stoichiometry of ZnO. Most importantly, the simulation of the Co^{2+} XPS spectra using charge-transfer multiplet calculations together with results from the XANES and KXSW analysis allows us to determine whether Co oxide precipitates into CoO rock salt phases or dilutes in the ZnO lattice. The second aim consists of proposing a way to tune the structural and electronic properties of the Co/ZnO system, which could then be applied to other metal/oxide interfaces. Thanks to processes activated by annealing, nanometer scale clusters grown on ZnO merge into larger islands. Further annealing induces the diffusion of Co into ZnO where it substitutes Zn atoms. The concentration profile of Co into the ZnO lattice is also tunable by the annealing temperature.

Received: September 14, 2010
Revised: February 18, 2011
Published: March 24, 2011

EXPERIMENT

Experimental Methods. The $(000\bar{1})$ surface of a ZnO single crystal produced by pressurized melt growth was polished by a mechanical and chemical method (NovaSic). The sample was then ultrasonically cleaned in dimethylsulfoxide and acetone and blown dry with nitrogen after each bath. After being loaded into an ultrahigh vacuum (UHV, base pressure $\approx 2 \times 10^{-9}$ mbar), it was cleaned by cycles of Ar^+ sputtering (1 keV, 5 min) and annealing (925 K, 20 min) until no more contaminants were detected by XPS and a sharp LEED pattern was observed. The sample was heated by direct current flow through a glassy carbon wafer in contact with the single crystal. The temperature was calibrated using a K type thermocouple in contact with the ZnO surface prior to cobalt deposition. Co (99.999% purity) was deposited from an electron beam evaporator. The deposition rate measured using a quartz oscillator before each deposition was between 0.016 and 0.075 nm per minute. The Co coverage is specified as equivalent thickness, i.e., as the thickness of an equivalent uniform layer of bulk Co with the same mass. The experimental data collected on the Co/ZnO system were also compared to measurements performed on a CoO single crystal, which was cleaned by Ar^+ sputtering (1 keV, 40 min).

The chemical interactions between Zn, Co, and O and the spatial distribution of these elements in the sample were studied by XPS and XANES. These measurements were performed at the X-ray wiggler beamline BW2 at HASYLAB, Hamburg, Germany.[6,7] For XPS, a photon energy of 3500 eV with a bandpass of 460 meV was selected. Photoelectrons were collected in normal emission geometry with the analyzer mounted 45° with respect to the polarization direction of the linearly polarized X-ray beam. The Au $4f_{7/2}$ peak at 84.0 eV binding energy (BE) recorded from a reference sample was used to calibrate the binding energy scale. To account for possible photon energy drifts due to changing heat load on the X-ray optical components, reference spectra were recorded before and after each core level and valence band data set. XANES measurements were performed by recording the total photoelectron yield; i.e., the sample drain current.

The position that Co atoms occupy in the ZnO host lattice was studied with the KXSW method.[8,9] The method is based on the properties of diffraction scattering and makes use of the X-ray standing wave, formed inside a crystal by coherent interference of incoming and Bragg diffracted waves.[10] In general, the standing wave period is equal to that of the diffracting planes and the phase depends on the deviation from the exact Bragg condition. The incident X-rays excite atoms inside the crystal and their fluorescence yield Y is proportional to the X-ray field intensity at the atom location. The movement of the nodes and antinodes of the wave field that follows the crystal rotation leads to variation of the fluorescence yield, and the form and amplitude of this variation can be used to detect the emitting atoms' positions in the host lattice unit cell. Only atomic shells with absorption edges below the energy of the incident beam E_0 contribute to the fluorescence signal, however, for a KXSW experiment E_0 can be freely chosen.

The ZnO crystals were not perfect enough for the conventional XSW approach, as the fast signal variation in the vicinity of the Bragg angle is blurred due to the mosaicity of the sample. Therefore, we have used the new kinematical XSW method, which uses the weak wave fields formed at large deviation from the Bragg condition. The method is very tolerant to lattice imperfections.

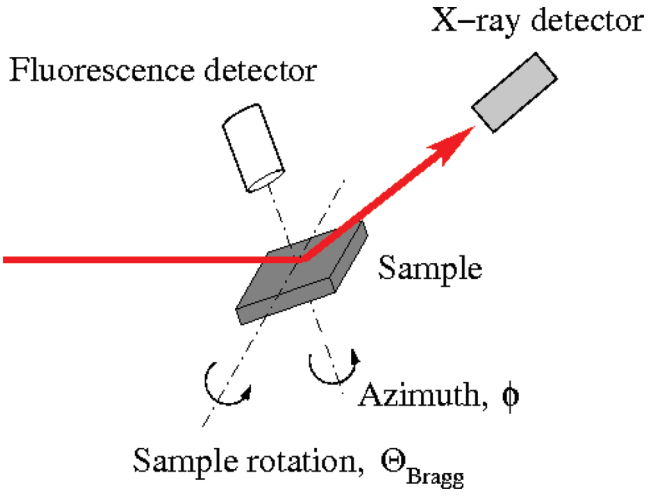

Figure 1. Schematic layout of the KXSW experiment at BW1. The normal to the Bragg scattering planes is aligned along the azimuthal rotation axis.

The KXSW measurements were carried out at the undulator beamlines BW1 at HASYLAB, Hamburg, Germany and ID32 at ESRF, Grenoble, France. A double-crystal Si(111) monochromator was used for wavelength tuning to the X-ray energies E_0 = 9.7 keV above the Zn K and Co K absorption edges and E_0 = 9.1 keV below the Zn K-edge for refinement of the cobalt atom position. The higher harmonics were suppressed by mirrors. A multiple-circle diffractometer allowed sample alignment with rotation around the Bragg plane reciprocal lattice vector for control of multiple reflection effects.[8] The Bragg scattering was detected with a scintillation counter, secondary fluorescence with a VORTEX silicon drift detector (Figure 1).

Theoretical Methods. Co 2p XPS spectra from cobalt monoxide in tetrahedral (wurtzite) and octahedral (rock salt) symmetry were simulated using the charge-transfer multiplet (CTM) approach which is described in detail elsewhere.[11] Calculations were performed using the CTM4XAS user interface.[12] This program is based on the Anderson model of the charge-transfer multiplets and provides simulation of X-ray absorption, photoelectron spectra of transition metal compounds. The calculated spectra were convoluted with a 0.3 eV wide (fwhm) Lorentzian to account for the core hole lifetime as well as with a 0.3 eV wide (fwhm) Gaussian to simulate the experimental energy resolution.

RESULTS

General Observations. Zn 2p, O 1s, and Co $2p_{3/2}$ XPS core level lines have been recorded at successive stages of the experiment (Figure 2). The relative energy alignment of the Zn 2p peaks compensates for band bending effects occurring upon cobalt deposition and allows for a clearer identification of changes in the peak line shape.

The line shape of the Zn 2p peak is not affected by the Co deposition and subsequent annealing. At higher binding energies weak satellites are observed (see inset in Figure 2) thanks to the high bulk sensitivity of high energy XPS. These features are attributed to bulk-related electronic excitation:[13,14] features A, B, and C are attributed to interband transitions from the filled O 2p and Zn 3d bands to the empty density of states in the conduction band while feature D is assigned to a collective excitation

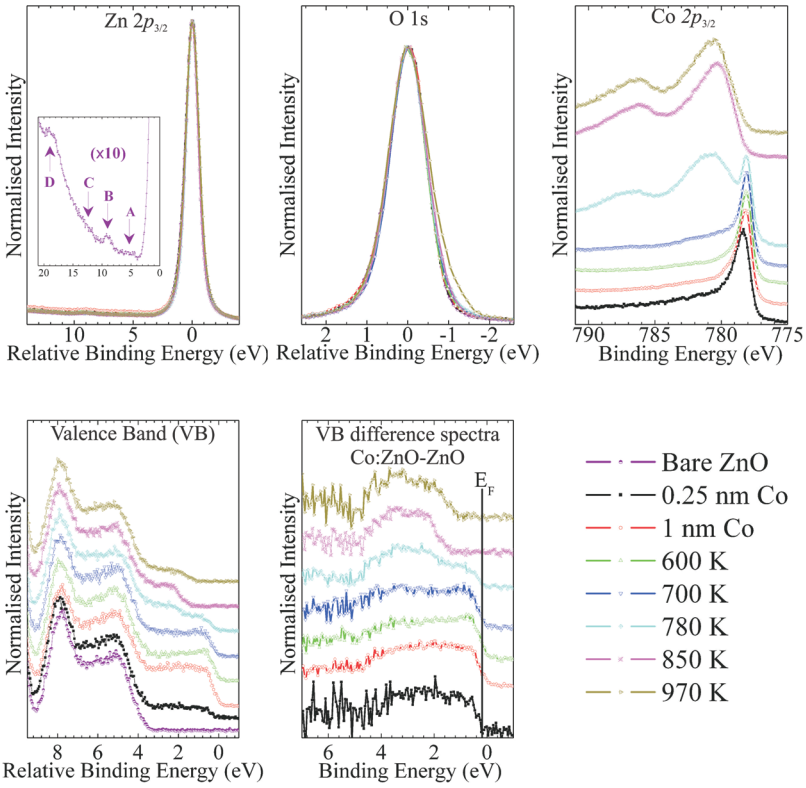

Figure 2. XPS spectra from Zn 2p, O 1s, Co 2p core levels and the ZnO valence band at successive stages of the experiment. The Zn 2p peak positions were aligned relative to their intensity maximum and an identical shift was applied to the corresponding O 1s peak. The inset shows the Zn 2p spectral region on an expanded scale. Features A, B, C, and D are described in the text. In valence band spectra, the Zn 3d related features (located 10.7 eV below E_F) were aligned on their maximum intensity to compensate for band bending effects. The last panel shows difference spectra obtained by subtracting a weighted valence band spectrum of bare ZnO from the aligned successive spectra (see text for details).

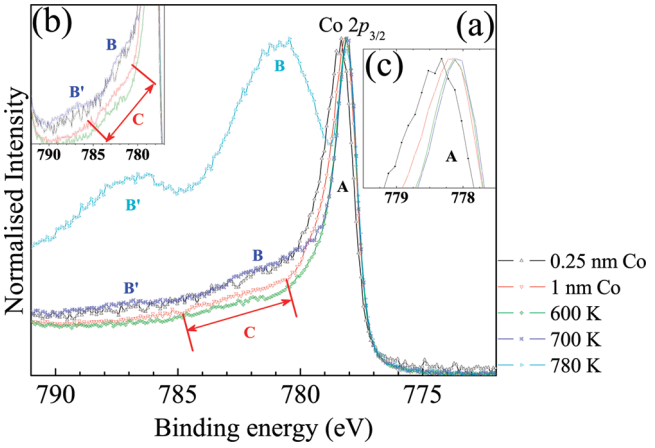

Figure 3. Co $2p_{3/2}$ XPS spectra after initial deposition and annealing. Insets show Co $2p_{3/2}$ spectral regions on an expanded scale. Features A−D are discussed in the text.

(plasmon) of O 2p and Zn 4s electrons. The line shape of O 1s spectra is also largely unaffected by the presence of cobalt except for a low energy component which appears upon annealing at 970 K.

During the growth process as well as after annealing at 600 K, the Co 2p line shape corresponds to that of metallic cobalt. Oxidation is initiated upon annealing at 700 K and results in several modifications of the Co 2p spectrum: a 3 eV shift to higher BE, a significant line broadening and the appearance of a pronounced charge-transfer satellite (at a BE of 787 eV), which will be discussed in more detail below. Metallic and oxidized cobalt coexist after annealing at 700 and 780 K but only oxidized Co remains at higher temperature.

The evolution of the valence band at the different stages of the experiment is also represented in Figure 2. As observed for Zn 2p, the line shape of Zn related features in the valence band is not affected by the experiment. To compensate for band bending effects, the spectra were aligned relative to the Zn 3d (not shown) peaks of bare ZnO appearing at a BE of 10.7 eV with respect to the Fermi level. This procedure allows us to better highlight the remaining spectral shape modifications and to extract these changes numerically from the raw data: difference spectra were derived by subtracting the valence band spectrum from the bare ZnO surface after suitable intensity scaling such that the difference is non-negative over the energy range of interest. This crude operation enhances the visibility of modifications to the valence electronic structure. Finally, the resulting difference spectra are presented in the last panel of Figure 2 using their original energy scale referred to the Fermi level.

As can be seen in valence band spectra, the metallic character of the Co density of states, which extends to the Fermi level, is preserved even after annealing at 700 K. At 780 K signatures from both metallic Co and Co^{2+} are observed. At higher temperatures, the valence band edge (Co 3d) moves away from the Fermi level by 1 eV, which is characteristic of Co^{2+} in ZnO.[15] Finally, the width of the Co 3d band in Co^{2+} seems to increase again after the

dx.doi.org/10.1021/jp108744c |J. Phys. Chem. C 2011, 115, 7411–7418

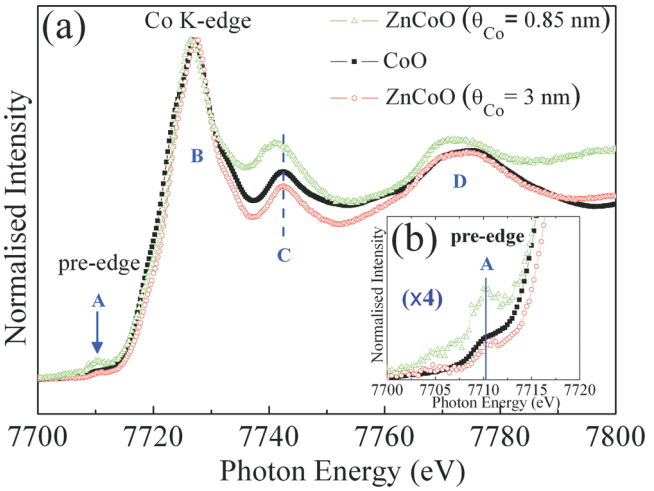

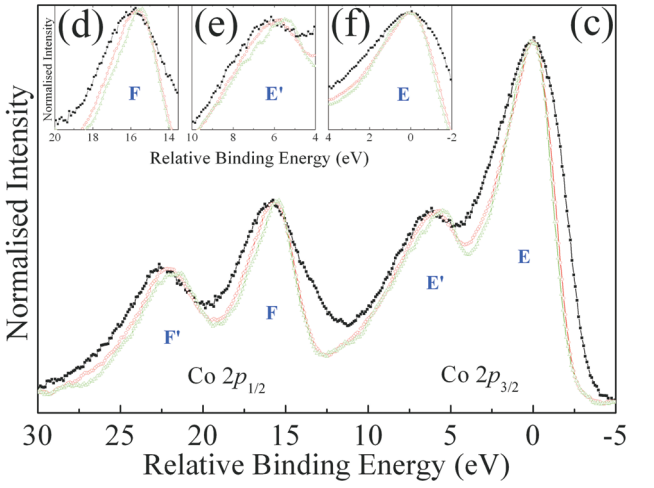

Figure 4. Comparison of Co *K*-edge XANES and Co 2p XPS spectra from a CoO single crystal and Co films (thickness 0.85 and 3 nm) grown on ZnO(000$\bar{1}$) and annealed at 970 K.

final annealing (970 K) where also a low BE component in the O 1s line shape is observed. As will be shown below, these two phenomena may have the same origin but cannot be solely associated to the oxidation of cobalt, which already occurs at much lower temperature (above 700 K). Additional experimental results will be provided in the following, which will help to interpret these two observations and to clarify the thermodynamical processes occurring during the annealing.

Structure of the Metallic Co Film. A close inspection of the Co 2p core level data reveals spectral information, helping us to understand how Co interacts with ZnO. Indeed, as explained in the following, the BE and width of the Co $2p_{3/2}$ peak are both tightly related to size effects. At first, from Figure 3a and insets b and c it is obvious that the Co 2p spectrum obtained after deposition of 0.25 nm is not only significantly broader than other curves (Figure 3 and inset c) but also shifted to higher BE. This is also often observed in photoemission from few-atom clusters and can be related to a weaker screening of the photohole.[16] After Co deposition of 1 nm, the Co $2p_{3/2}$ peak narrows and shifts to lower BE. This trend proceeds even further upon annealing at 600 K, indicating a gradual loss of the size effect along these successive steps.

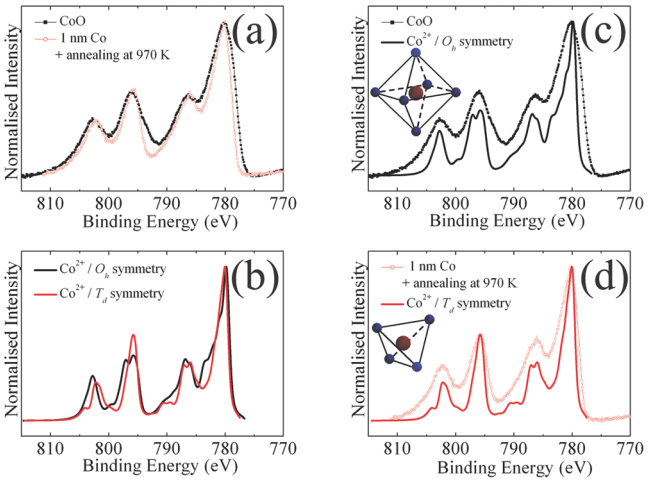

Figure 5. (a) Co 2p XPS spectra from a CoO single crystal and a 1 nm thick Co film grown on ZnO(000$\bar{1}$) and annealed at 970 K. The experimental spectra are compared to theoretical XPS spectra calculated for octahedral (c) and tetrahedral (d) coordination of the Co^{2+} ion. The comparison of both calculated spectra is shown in (b).

The spectral region indicated by C in Figure 3a and inset b corresponds to the location where a satellite was reported by Nath et al.,[17] which is related to the existence of different channels for screening the hole from the Co 2p level. This low-intensity feature is characteristic of small clusters and not observed for bulk materials.[18] In our case, it appears to be very weak in spectra from samples with low Co coverage and to disappear altogether after annealing.

In summary, the first three stages of this experiment indicate that nanometer sized clusters are initially formed, likely due to the poor adhesion of Co onto ZnO. The successive reduction and disappearance of size effects in the spectra are indicative of larger clusters, i.e., that the clusters coalesce upon the increase in Co amount and annealing temperature. These observations are in good agreement with a previous work from our group where the nucleation of Co clusters on ZnO and their coalescence upon annealing was observed by STM.[19]

Annealing at 700 K leads to the appearance of two satellites labeled B and B′ (Figure 3 and inset b) attributed to the beginning of the oxidation process, since these satellites appear at the same energy as the main lines from cobalt in the 2+ oxidation state which becomes dominant after annealing at 780 K. The oxidation of Co is discussed in the following section.

Co Oxidation. In the present study, the Co oxide formed by annealing at a temperature higher than 600 K contains cobalt in a 2+ oxidation state as in CoO. This is concluded from the similar line shapes of the Co K-edge XANES and Co 2p XPS spectra (Figure 4a,c) from Co films grown on ZnO and annealed at 970 K (named (Zn,Co)O in the following) and from a CoO single crystal.

In Figure 4a, the Co K-edge XANES spectra from two (Zn, Co)O films (prepared with an initial Co amount of 0.85 nm respectively 3 nm) are compared to the spectrum from a CoO single crystal. The pre-edge feature A (inset b) arises from 1s to 3d multipole transitions mediated by the Co 3d−O 2p covalency. The absence of any additional feature in the pre-edge indicates that no metallic Co is present in the samples within the detection limit of a few atomic percent.[15]

dx.doi.org/10.1021/jp108744c |J. Phys. Chem. C 2011, 115, 7411–7418

Table 1. Best Parameter Sets Extracted from Charge-Transfer Multiplet Calculations

symmetry	$10Dq$	Δ	U_{dd}	U_{pd}	T_σ	T_π
O_h	1.8	4.0	7.0	8.5	1.75	1
T_d	−1.2	4.0	7.0	8.5	1	1.6
T_d[21]	−0.7	5.0	6.0	8.5	1	2.16

The Co K-edge XANES spectra of Co^{2+} in CoO and (Zn, Co)O are similar, in agreement with Kaspar et al.[15] Nonetheless, when the spectra obtained for (Zn,Co)O are compared, it appears that in the case of the smaller initial Co amount feature A is stronger, feature C is broader and shifted toward lower photon energy while feature D is narrower. As shown recently,[20] pre-edge feature A is much more intense in tetrahedral than in octahedral coordination. Cobalt ions in CoO (NaCl structure) are octahedrally coordinated while Co substituting Zn atoms in ZnO (wurtzite structure) are tetrahedrally coordinated. This would imply that, when the initial (i.e., prior to annealing) amount of cobalt is relatively small ($\theta \leq 1$ nm), Co is thermally incorporated into the ZnO wurtzite lattice where it substitutes Zn, while for a larger initial Co amount, a secondary rock salt CoO phase is preferentially formed after annealing.

As seen in Figure 4c (and insets d−f), the shape of the Co 2p XPS spectra is also affected by the initial Co amount: the apparent spin−orbit splitting (energy separation between feature E and F), the charge-transfer splitting (energy separation between feature E and E'), and the width of the lines all increase for larger initial Co amount. Before providing an interpretation for this trend, the origin of these features is briefly recalled. The oxidation of Co leads to the appearance of a double peak structure due to the existence of multiple final states associated with charge transfer between Co and neighboring O ligands. Indeed, the initial electronic configuration of Co^{2+} is d^7. Following the photoemission process, the photohole on the Co 2p core level is screened by valence electrons. The screening may be increased by additional charge transfer from ligand atoms (oxygen) to the cobalt. As a result, multiple final states may coexist, giving rise to satellite structures. The two broad features E and E' in Figure 4c reflect the energy range of the principal configurations cd^7, cd^8L, and cd^9L^2, where c denotes the core hole, d^n is the presence of n electrons in the d shell, and L^m is the number m of holes on the ligand 2p orbital after electron transfer. The line shape of features E and E', their relative energy splitting, and their intensity ratio is mostly affected by the Co oxidation state. In addition, the crystal field symmetry might also affect the fine details of the line shape since features E and E' constitute the envelope of a multiplet structure arising from the various electronic configurations within the open d shell for each of the principal configuration. The Co 3d shell is split into low energy t_{2g} (respectively e) and high energy e_g (respectively t_2) levels for octahedral (respectively tetrahedral) crystal field symmetry. The various possibilities of filling the available d electrons into these levels lead to multiple energy states that can additionally be split by spin−orbit coupling with the core 2p hole.

In the following we aim to establish whether the modifications observed in the Co 2p XPS spectra with increasing Co amount could result from different (i.e., tetrahedral or octahedral) crystal field symmetries around Co atoms. We performed calculations based on the charge-transfer multiplet (CTM) model and compared the experimental spectra (Figure 5a) from a rock salt CoO single crystal and (Zn,Co)O with the calculated spectra for octahedrally and tetrahedrally coordinated Co^{2+} (Figure 5b). The Co^{2+} spectra were calculated using the CTM4XAS program described above, which includes cd^7 and cd^8L configurations. The finite crystal temperature (300 K) is included in the calculation through a Boltzmann distribution of the occupation of the initial states. Table 1 contains parameter sets referring to the spectra shown in Figure 5b and from Kobayashi's atomic multiplet simulations of Co 2p spectra obtained on (Zn,Co)O epilayers.[21] $10Dq$ refers to the crystal field splitting. It takes negative (respectively positive) values for tetrahedral (respectively octahedral) symmetry. Δ is the charge-transfer parameter, U_{dd} is the Hubbard U d−d repulsion energy, U_{pd} is the core hole potential, and T_σ (respectively T_π) is the hybridization energy between the metal $d_{3z^2-r^2}$ or $d_{x^2-y^2}$ (respectively d_{xy}, d_{yz}, or d_{zx}) and the ligand p orbitals. As shown by Bocquet and Fujimori,[22] there is no unique set of parameters leading to a proper fit of the experimental data. Hence, to simulate the data in a consistent way, we first tried to match both the intensity ratio and energy splitting between the main $2p_{3/2}$ line and its charge-transfer satellite. In the case of O_h symmetry, we assume that Co^{2+} is in a high spin state and refer to Bocquet's look-up tables[22] to define a set of initial parameters. These parameters are then slightly modified for a better match of our data. The final adjustment consists in tuning the crystal field energy $10Dq$ inside a window ranging from 0.5 to 2.0 eV. In the case of T_d symmetry, we use the best parameter set obtained for O_h symmetry as initial parameter set, except that the sign of $10Dq$ is changed and that the values for T_π and T_σ are exchanged. Finally, we tune the value of $10Dq$ and T_π to reach the best match between the calculated and experimental spectra. The parameter sets extracted from this procedure, although slightly different from Kobayashi's,[21] are in fair agreement with Bocquet's look-up tables. We notice that the hybridization energy and crystal field splitting are slightly smaller in the T_d symmetry.

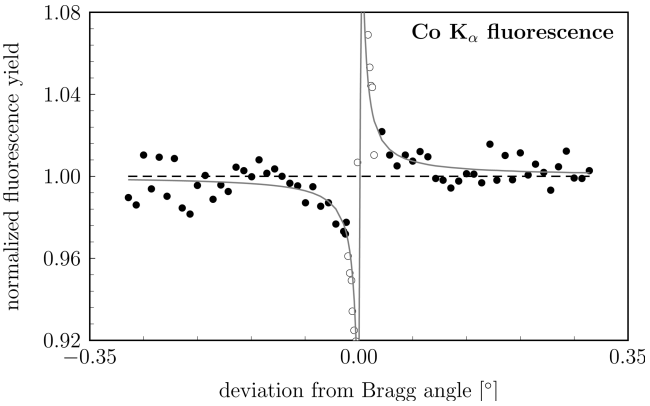

Figure 6. Co Kα fluorescence yield (dots) and theoretical curve (solid line) in the vicinity of the ZnO (002) Bragg reflection at 9.1 keV. Only the black data points were used for the kinematical data evaluation.

In the experimental spectra displayed in Figure 5a, there are differences between the Co 2p lines from rock salt CoO and tetrahedrally coordinated Co^{2+} ions. As seen in Figure 5b−d, the simulated spectra reproduce the experimental trend, especially a slight broadening of the Co 2p main lines in the O_h symmetry. However, on the basis of this alone, we can hardly conclude for one symmetry or the other.

In summary, the analysis of the experimental and simulated XPS spectra reveals that very little difference exists between the spectral signature from rock salt and wurtzite Co^{2+}. XANES data

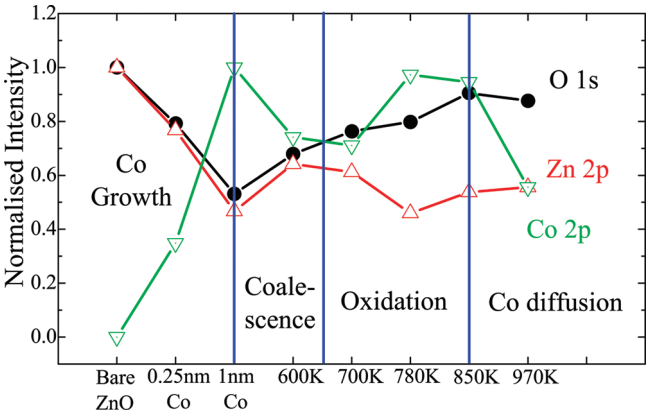

Figure 7. Changes in the Zn 2p, O 1s, and Co 2p line intensity at the different stages of the experiment. Zn 2p and O 1s signals are normalized with respect to their value on the bare ZnO surface. Co 2p is normalized for 1 nm Co.

provide a fair indication that for a relatively small initial Co amount, Co atoms are preferentially substituting Zn atoms in the wurtzite structure. Nonetheless, to further establish the location of the Co atoms, we resorted to KXSW analysis.

Cobalt Atom Position in the ZnO Lattice. A typical Co Kα fluorescence yield curve is presented in Figure 6.

The experimental data are obtained from a sample after the heat treatment procedure as described above, to ensure that the Co is diffused into the ZnO and oxidized. The solid line is the fit to the fluorescence yield at the tails of the diffraction curve (black dots). The data in the area where the kinematical diffraction theory cannot be applied (open circles) are excluded from the analysis.

The position of the Co atoms can be found from the fluorescence yield $Y(\Delta\theta)$:

$$Y(\Delta\theta) \propto 1 + \frac{\Gamma}{\sin 2\theta_B} \mathscr{Y}_c \frac{1}{\Delta\theta} \qquad (1)$$

with the atom position dependent parameter

$$\mathscr{Y}_c = |F_H| f_c \cos(2\pi\Phi_c - \arg F_H) \qquad (2)$$

where the coherent position Φ_c describes the average position of the impurity atoms measured relative to the diffraction planes and the coherent fraction f_c corresponds to the spread of these atoms around the average position. $|F_H|$ and arg F_H are absolute value and phase of the structure factor of ZnO.

The parameter $\mathscr{Y}_c = 38 \pm 2$ obtained from the experimental data corresponds to Co atoms occupying the host Zn atoms position, which is consistent with results obtained by other authors.[15] The presence of Co atoms at interstitial positions or oxygen sites may thus be excluded, although the experimentally obtained value is lower than the theoretical value $\mathscr{Y}_{c,theo} = 39.95$. Furthermore, it is interesting to calculate the coherent fraction within the single position model (i.e., Co at the Zn position), which yields $f_c = \mathscr{Y}_c/\mathscr{Y}_{c,theo} = 0.95 \pm 0.05$. This value is slightly less than unity, which is typical for crystalline matter with a high degree of lattice perfection but small random displacements due to local atomic disorder. The coherent fraction is then identical with the Debye–Waller factor $D_H = e^{-1/2\langle(\mathbf{H}\cdot\mathbf{u})^2\rangle}$. From that a mean displacement $(\langle u_z^2\rangle)^{1/2} = 0.013 \pm 0.007$ nm of the Co atoms from the Zn position can be determined. Thus, the KXSW

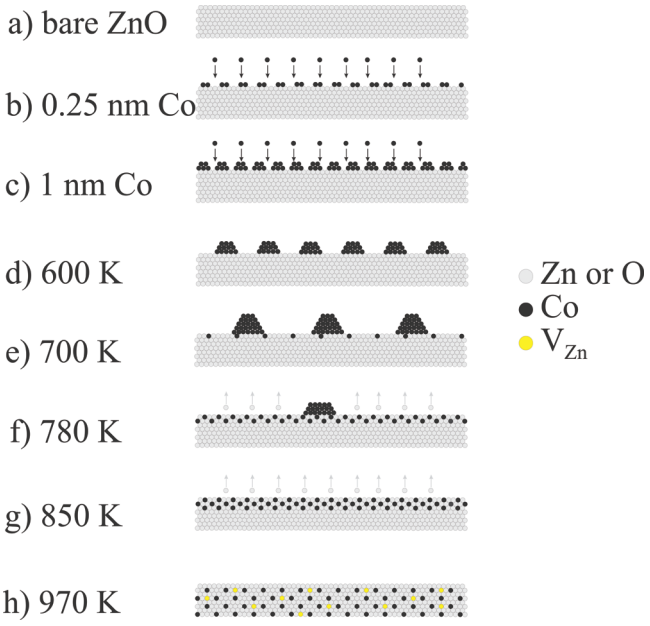

Figure 8. Model showing the various stages of the structural modifications during the growth and annealing of the Co/ZnO system.

results confirm the XANES data and additionally justify the choice of atomic configuration models used for the calculated XPS spectra.

Scenario of the Co/ZnO Interface Transformation. In the previous sections, several thermally activated processes have been discussed on the basis of the analysis of the XPS and XANES spectral features. Relative intensity changes in the Zn 2p, O 1s, and Co 2p XPS core level lines (Figure 7) can also be related to reorganization of the film constituents. From the interpretation of these changes and conclusions drawn in the previous sections, we propose a scenario of the film transformation that is explained in the following and illustrated in Figure 8.

Four distinct stages can be identified (Figure 7). At first, the growth of the 1 nm thick film induces a decrease of the ZnO related lines and an increase of Co 2p with the amount of Co deposited. As discussed above, at this point the Co film shows signs of size effects that fade out with increasing film thickness. This is attributed to Co aggregation into nanometer scale clusters (Figure 8a–c). Then, after annealing at 600 K, the Co 2p intensity decreases while the intensities of O 1s and Zn 2p increase (Figure 7). It was also concluded from the Co 2p line shape that Co remains mostly metallic and the size effects disappear (see above). This indicates that the Co clusters coalesce into larger islands between which the ZnO surface is again uncovered (Figure 8d–e).

In the temperature range between 700 and 850 K, the 1:1 Zn:O stoichiometry is lost and a depletion of Zn is observed (Figure 7). At this stage, it is also seen that Co is becoming gradually fully oxidized. Hence, we believe that Co progressively diffuses into the ZnO subsurface where it substitutes Zn. The substituted Zn probably migrates toward the surface and desorbs (Figure 8f,g).

Finally, when the annealing temperature exceeds 850 K, the Co 2p signal decreases (Figure 7). This may be explained by Co diffusing deeper into ZnO. The bulk solubility of Co into ZnO is in principle very low (below 1% at room temperature[23]) but the formation energy of Co_{Zn} defects (Co substituting Zn atoms)

decreases in the vicinity of the surface, which explains the oxidation process mentioned earlier.[24] The bulk solubility limit of Co in ZnO also increases in relation with the annealing temperature.[25] Hence, dilution of Co and its diffusion deeper into the bulk of ZnO is favored by annealing.

As mentioned above, the O 1s line shape changes after the final annealing at 970 K. It can therefore not solely be related to the oxidation process, which is already complete at 850 K. In addition, such features in the O 1s XPS line shape related to Co oxidation have not been reported in the literature about (Zn, Co)O ternary compounds. The change in the O 1s line shape could also be related to the precipitation of Co into a CoO phase where each O atom is bound mostly to Co atoms whereas in diluted (Zn,Co)O, O atoms are bound to one Co atom at maximum. In such a case, the local electronic structure at the O atoms in CoO would be more strongly perturbed by the electronegativity difference between Co and Zn. Nevertheless, the formation of a CoO rock salt secondary phase was ruled out for such a small (1 nm) initial Co amount by the present XPS, XANES, and KXSW measurements. Finally, the precipitation of Co into a CoO wurtzite phase is not compatible with the drop of the Co 2p line intensity observed at 970 K (Figure 7).

Therefore, the change in the O 1s line shape at 970 K requires another interpretation. Diffusion of Co into ZnO may proceed in various ways. In the present work, evidence is provided that Co diffuses via Zn substitution because, above 780 K, Co is always found in a 2+ oxidation state. Hence, when Co^{2+} leaves a subsurface site to diffuse deeper into the bulk of ZnO, Zn vacancies are likely to be created at the previous Co sites (Figure 8h).

Zn vacancies constitute very mobile defects under *n*-type doping[26] and create acceptor levels located 0.9 eV above the ZnO valence band edge.[27] As the ZnO single crystals used in this study are *n*-type, these acceptor levels are filled with electrons. The electronic structure of O atoms in the vicinity of Zn vacancies is therefore strongly perturbed: each of the four atoms surrounding this vacancy has an extra half electron. We believe that the low binding energy feature observed on the O 1s line and the spreading of the valence band edge toward the Fermi level (Figure 2) could both be related to a high density of subsurface Zn vacancies created after the diffusion of Co deeper into the bulk. However, additional experimental evidence from, e.g., photoluminescence data would be required to confirm this hypothesis.

CONCLUSIONS

The combination of high energy X-ray based techniques allowed us to elucidate the complex processes occurring when annealing an ultrathin Co film grown on a ZnO$(000\bar{1})$ single crystal. When the annealing temperature remains below 700 K, the nanometer scale clusters from the Co film remain metallic and coalesce. Above that temperature, oxidation starts to proceed via Zn substitution. When the annealing temperature reaches 970 K, Co^{2+} ions diffuse deeper into the bulk of the ZnO single crystal. Following this diffusion, Zn vacancies are formed in the vicinity of the surface at sites previously occupied by Co atoms. From a technological point of view, this study shows that the structural properties of this metal/oxide interface can be thermally tuned to provide a wide variety of interesting systems (Figure 8) ranging from nanometer scale clusters showing size-dependent electronic structure relevant, e.g., for catalytic applications to ternary metal oxides with various levels of Co concentration. From a more fundamental point of view, a deeper insight has been gained on the processes associated with the substitution of Zn atoms by Co and with the dilution of Co into the ZnO lattice.

AUTHOR INFORMATION

Corresponding Author
*E-mail: jacques.dumont@fundp.ac.be.

ACKNOWLEDGMENT

We thank W. Caliebe for providing a CoO crystal. This work was supported by the Belgian Fund for Scientific Research (FNRS-FSR), by the Belgian Office for Scientific, Technical and Cultural Affairs (PAI 5.01) and by DESY and the European Community's Seventh Framework Programme (FP7/2007-2013) under grant agreement no. 226716. J.A.D. and J.G. are respectively postdoctoral researcher and research associate from the Belgian National Fund for Scientific Research (NFSR).

REFERENCES

(1) Campbell, C. *Surf. Sci. Rep.* **1997**, *27*, 1.
(2) Pan, F.; Song, C.; Liu, X.; Yang, Y.; Zeng, F. *Mater. Sci. Eng. R* **2008**, *62*, 1.
(3) Tsukazaki, A.; Ohtomo, A.; Kita, T.; Ohno, Y.; Ohno, H.; Kawasaki, M. *Science* **2007**, *315*, 1388.
(4) Hyman, M.; Martono, E.; Vohs, J. *J. Phys. Chem. C* **2010**10.1021/jp9103883.
(5) Xie, W.; Xie, F.; Yu, X.; Xue, K.; Xu, J.; Chen, J.; Zhang, R. *Appl. Phys. Lett.* **2009**, *95*, 262506.
(6) Drube, W.; Schulte-Schrepping, H.; Schmidt, H.-G.; Treusch, R.; Materlik, G. *Rev. Sci. Instrum.* **1995**, *66*, 1668.
(7) Drube, W. *Nucl. Instrum. Methods Phys. Res., Sect. A* **2005**, *547*, 87.
(8) Tolkiehn, M.; Novikov, D.; Fanchenko, S. *Phys. Rev. B* **2005**, *71*, 165404.
(9) Tolkiehn, M.; Novikov, D. V. *The X-ray Standing Wave Technique: Principles and Applications*; World Scientific: Singapore, 2010; in production.
(10) Zegenhagen, J. *Surf. Sci. Rep.* **1993**, *18*, 202.
(11) de Groot, F.; Kotani, A. *Core Level Spectroscopy of Solids*; Taylor & Francis Group, CRC Press: Bocca Raton FL, 2008.
(12) Stavitski, E.; de Groot, F. M. F. *Micron* **2010**, *41*, 687.
(13) Hengehold, R.; Almassy, R.; Pedrotti, F. *Phys. Rev. B* **1970**, *1*, 4784.
(14) Dorn, R.; Lüth, H.; Büchel, M. *Phys. Rev. B* **1977**, *16*, 4675.
(15) Kaspar, T. C.; Droubay, T.; Heald, S. M.; Nachimuthu, P.; Wang, C. M.; Shutthanandan, V.; Johnson, C. A.; Gamelin, D. R.; Chambers, S. A. *New J. Phys.* **2008**, *10*, 055010.
(16) Citrin, P.; Wertheim, G. *Phys. Rev. B* **1983**, *27*, 3176.
(17) Nath, K.; Haruyama, Y.; Kinoshita, T. *Phys. Rev. B* **2001**, *64*, 245417.
(18) Klebanoff, L. E.; Van Campen, D. G.; Pouliot, R. J. *Phys. Rev. B* **1994**, *49*, 2047.
(19) Dumont, J.; Mugumaoderha, M. C.; Seldrum, T.; Frising, F.; Moisson, C.; Turover, D.; Sporken, R. *J. Vac. Sci. Technol. B* **2007**, *25*, 1536.
(20) de Groot, F.; Vankó, G.; Glatzel, P. *J. Phys.: Condens. Matter* **2009**, *21*, 104207.
(21) Kobayashi, M.; Ishida, Y.; Hwang, J.; Mizokawa, T.; Fujimori, A.; Mamiya, K.; Okamoto, J.; Takeda, Y.; Okane, T.; Saitoh, Y.; Muramatsu, Y.; Tanaka, A.; Saeki, H.; Tabata, H.; Kawai, T. *Phys. Rev. B* **2005**, *72*, 201201.

(22) Bocquet, A.; Fujimori, A. *J. Electron Spectrosc. Relat. Phenom.* **1996**, *82*, 87.
(23) Bates, C.; White, W.; Roy, R. *J. Inorg. Nucl. Chem.* **1966**, *28*, 397.
(24) Chen, X.; Huang, D.; Deng, W.-J.; Zhao, Y.-J. *Phys. Lett. A* **2009**, *373*, 391.
(25) Straumal, B.; Mazilkin, A.; Protasova, S.; Myatiev, A.; Straumal, P.; Baretzky, B. *Acta Mater.* **2008**, *56*, 6246.
(26) Huang, G.-Y.; Wang, C.-Y.; Wang, J.-T. *Solid State Commun.* **2009**, *149*, 199.
(27) Janotti, A.; Van de Walle, C. *J. Cryst. Growth* **2006**, *287*, 58.